Statistical properties of the radiation from VUV FEL at DESY operating at 30 nm wavelength in the femtosecond regime

E.L. Saldin, E.A. Schneidmiller, and M.V. Yurkov

Deutsches Elektronen-Synchrotron (DESY), Hamburg, Germany

Abstract

Since spring, 2005 vacuum ultraviolet free electron laser (VUV FEL) at DESY operates as user facility in the wavelength range around 30 nm. Electron beam formation system at the VUV FEL is essentially nonlinear and naturally results in a formation of a short high-current leading peak in the density distribution that produces FEL radiation. The main feature of the femtosecond mode of operation of the VUV FEL is the production of short, down to 20 fs radiation pulses with GW-level peak power. This paper is devoted to detailed studies of the short-pulse effects in the VUV FEL at DESY operating in the femtosecond regime, and to analysis of first experimental results.

1 Introduction

The project of the VUV FEL at DESY is realized in two phases. Phase I (1999-2002) served for a proof-of-principle of SASE FEL operation and for system tests of the hardware. Phase II of the VUV FEL has been built as an extension of phase I to shorter wavelengths (down to 6 nm) and is used as the first VUV FEL user facility starting in spring, 2005. The nominal design of the VUV FEL assumes a linearized compression of the electron bunch in two bunch compressors with the help of the 3rd harmonic superconducting RF cavity [1]. This would allow to prepare electron bunch with relatively long lasing part and to reach original specifications for the output radiation in terms of pulse duration, of about 200 fs FWHM. Longer pulse duration is required for user applications exploiting high average brilliance, or photon flux. On the other hand, there is a strong interest of the user community in shorter radiation pulses for time-resolved experiments.

VUV FEL Phase I demonstrated unique femtosecond mode of operation [2,3] which was not considered at an early design stage of the project [4]. Thorough

Preprint submitted to Nucl. Instrum. Meth. A

analysis has shown that due to nonlinear compression and small local energy spread the short high-current (3 kA) leading peak (spike) in the bunch density distribution was produced by beam formation system. Despite strong collective effects (of which the most critical was the longitudinal space charge after compression) this spike was bright enough to drive FEL process up to the saturation for the wavelengths around 100 nm [5]. In addition to the possibility for production of high-power femtosecond pulses this mode of FEL operation demonstrated high stability with respect to drifts of machine parameters.

Successful operation of the VUV FEL Phase I in the femtosecond regime encouraged us to extend such a mode of operation for shorter wavelengths. Relevant theoretical study has been performed in [6]. It has been found that the beam formation system of the linac can be tuned for production of bunches with a high-peak-current spike capable for effective driving of the FEL process such that the VUV FEL can safely saturate even at the shortest design wavelength of 6 nm with a GW level of the peak power in short pulses of 15-100 fs duration.

Optimum range of parameters suggested in [6] has been chosen for the commissioning of the VUV FEL. First experimental results obtained at the VUV FEL operating at the radiation wavelength around 30 nm have shown good agreement with predictions [7]. Commissioning of the VUV FEL proceeded in parallel with first user experiments. Our contacts with user community shows that planning of future user experiments at the VUV FEL requires more detailed knowledge of the expected statistical properties of the radiation source, and present paper fills this gap.

2 Formation of the electron bunch

Schematic layout of the VUV FEL (status for the year 2005) is shown in Fig. 1 [1]. The electron beam is produced in a rf gun and accelerated up to 700 MeV by five cryomodules ACC1-ACC5. At energy levels of 130 and 380 MeV the electron bunches are compressed in the bunch compressors BC1 and BC2. The undulator is a fixed 12 mm gap permanent magnet device, period length is

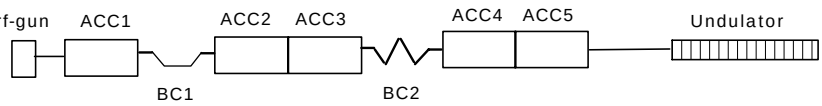

Fig. 1. Schematic layout of the VUV FEL (status for year 2005). Abbreviations ACC and BC stand for accelerating module and bunch compressor, respectively

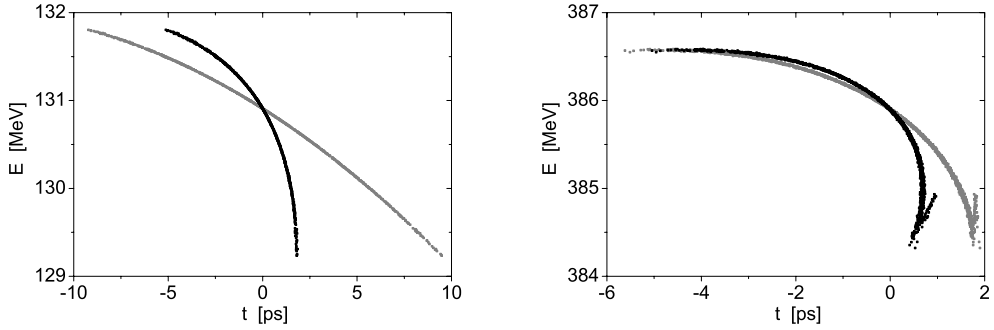

Fig. 2. Schematic illustration of two-stage nonlinear bunch compression. Phase space distribution of the electrons before (grey dots) and after bunch compressors BC1 (left plot) and BC2 (right plot). Bunch head is at the right side

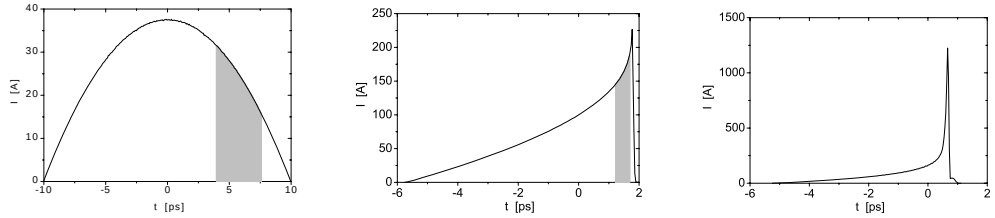

Fig. 3. Schematic illustration of two-stage nonlinear bunch compression. Current distribution along the electron bunch after accelerating module ACC1, bunch compressors BC1, and BC2 (left, middle, and right plot, respectively). Grey area on the left and middle plots shows part of the bunch compressed to high current spike after BC2 (right plot). Bunch head is at the right side

2.73 cm and peak magnetic field is 0.48 T. The undulator system is subdivided into six segments, each 4.5 m long. An important difference from the final setup [1] is that the 3rd harmonic rf cavity is not installed yet. Thus, beam formation system is essentially based on the use of nonlinear compression. This naturally leads to formation of asymmetrically shaped electron bunches with a sharp high current spike on a 100 fs scale duration. At a proper optimization of the bunch compression system it is possible to preserve small value of the emittance in the current spike. Bunch formation system of the VUV FEL operating in the femtosecond regime has been studied in details in [6]. We considered two possible options of operation: with a nominal charge of 0.5 nC, and with higher charge, of 1 nC. Both options can be realized experimentally and provide different modes of the VUV FEL operation in terms of output characteristics of the radiation.

Operation of the nonlinear bunch compression system realized at the VUV FEL is illustrated schematically with plots presented in Figs. 2 and 3. The electron beam originating from the electron gun is relatively long ($1.5-2$ mm rms) with respect to the rf-wave length (23 cm). When the bunch is accel-

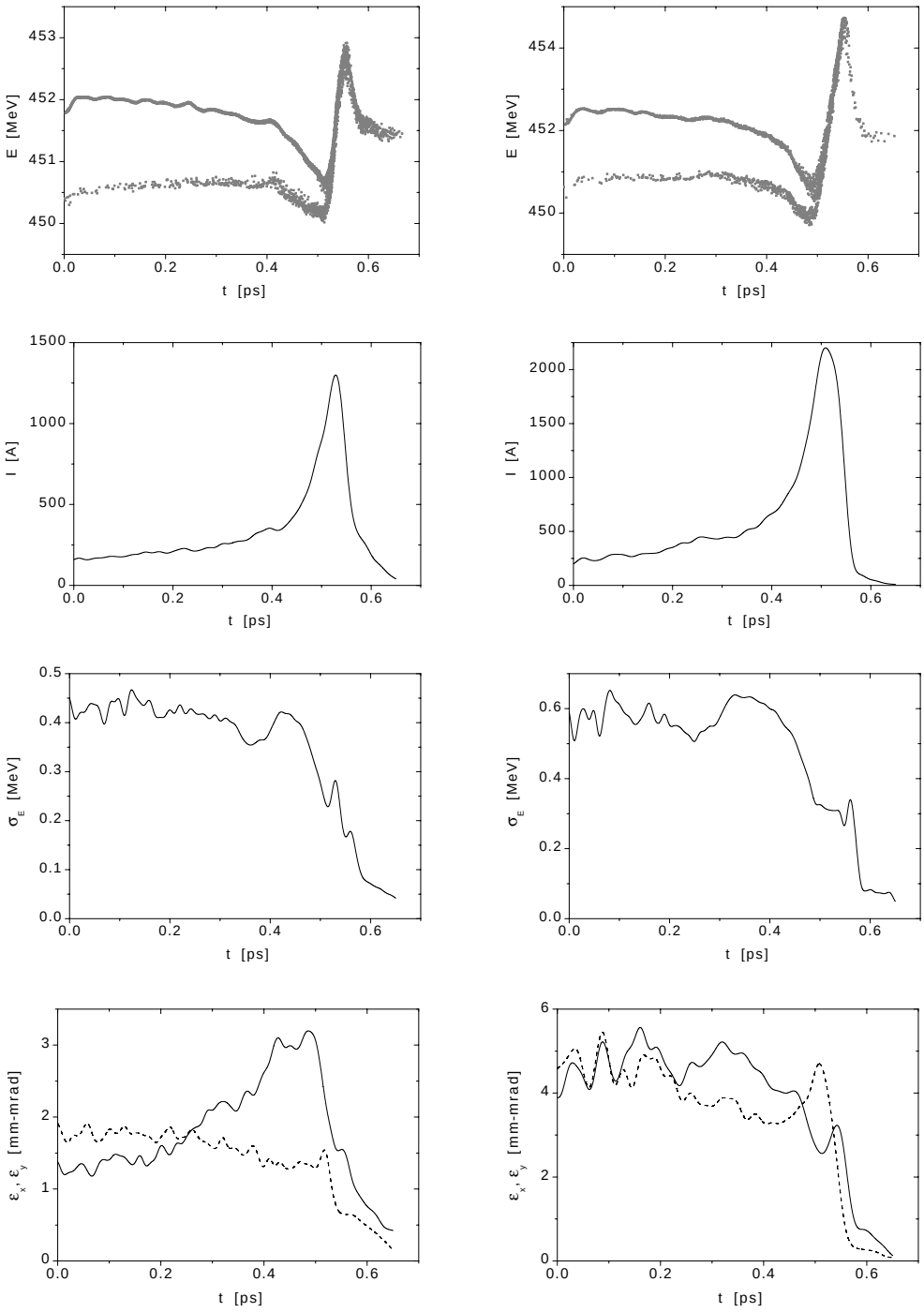

Fig. 4. Phase space distribution, current, slice emittance and slice energy spread along the bunch at the undulator entrance. Left and right columns correspond to the of 0.5 and 1 nC, respectively. Bunch head is at the right side

erated off-crest in the accelerating module ACC1, longitudinal phase space accumulates an rf-induced curvature. This distortion results, downstream of the bunch compressor, in a non-Gaussian distribution with a local charge con-

centration.

In fact, collective effects play significant role in the bunch compression process for short pulses. For high-current part of the bunch with rms length σ_z and peak current I coherent synchrotron radiation (CSR) and longitudinal space charge (LSC) effects scale as $\sigma_z^{-1/3}$ and σ_z^{-1}, respectively. For instance, LSC-induced energy chirp along the high-current spike of the bunch grows when the bunch travels from the bunch compressor to the undulator entrance [5]:

$$\frac{d(\Delta\gamma)}{dz} \simeq 2.4 \, \frac{I}{I_{\rm A}} \, \frac{\ln(\gamma\sigma_z/\sigma_\perp)}{\sigma_z\gamma^2} \, , \tag{1}$$

where $I_{\rm A} = 17$kA is the Alfven current, γ the relativistic factor and $\sigma_\perp$ the rms transverse size of the electron bunch.

Target goal for the FEL is high value of peak current keeping slice emittance and energy spread at a low level. Also, energy chirp along the bunch should not be too large in order to prevent gain degradation and increase of the spectrum width. In order to tolerate collective effects, a procedure of two-stage compression has been developed which allows to produce electron bunches with good lasing properties (see Figs. 2 and 3) [6]. Calculations have been performed with the codes Astra [8] and `elegant` [9]. Starting from peak current of 30-50 A at the exit of accelerating module ACC1, a mild compression is performed in the bunch compressor BC1, and then a high-current spike (containing about $10-15\%$ of the total charge) is formed in the bunch compressor BC2. Combination of rf phases in accelerating modules ACC1, ACC2, and ACC3 defines a slice in the initial distribution of which the spike is formed (see Fig. 3). Optimum parameters of the electron bunch at the undulator entrance are shown in Fig. 4. It is the head of the bunch with a high peak current which is capable to drive the lasing process. Complicated phase space distribution of the electrons in the head of the bunch is mainly due to the action of the longitudinal space charge field.

3 Parameter space of the VUV FEL

General overview of expected output characteristics of the VUV FEL has been presented in our previous paper [6]. Here we perform more detailed analysis of the features of the radiation related to ultra-short pulse duration. Slice properties of the bunch at the undulator entrance demonstrate rather complicated behavior (see Fig. 4). Evidently, a high current spike in the head of the bunch has preference for light amplification because of higher value of peak current and smaller emittance. Parameters of the spike are as follows: peak current is $1-2$ kA, FWHM length of high current spike is $20-30$ μm, and normalized

emittance $1.5 - 3.5$ mm-mrad for bunch charge $0.5 - 1$ nC. Prior presentation of simulation results it is useful to perform analysis of parameter space of the VUV FEL. As a zero order approximation we use simple one-dimensional estimations in terms of the FEL parameter ρ [13,14]:

$$\rho = \left[\frac{I}{I_{\rm A}} \frac{A_{JJ}^2 K^2 \lambda_{\rm w}^2}{32\pi^2 \gamma^2 \epsilon_n \beta_{\rm f}} \right]^{1/3} .$$

Here $\lambda_{\rm w}$ is undulator period, K is rms undulator parameter, γ is relativistic factor, $I_A = mc^3/e \simeq 17$ kA, $(-e)$ and m are charge and mass of electron, ϵ_n is normalized rms emittance, and $\beta_{\rm f}$ is focusing beta function in the undulator. Coupling factor is $A_{JJ} = [J_0(Q) - J_1(Q)]$, where $Q = K^2/[2(1 + K^2)]$, and K is rms undulator parameter. For focusing beta function in the undulator of 4.5 m slice parameters in the current spike result in the value of the FEL parameter $\rho = 2.5 - 3 \times 10^{-3}$. Thus, spectrum width generated by a slice of the electron beam is expected to be about $\Delta\omega/\omega \simeq \rho \simeq 0.5\%$. Lasing part of the bunch has relatively strong energy chirp. First consequence of the energy chirp is extra widening of the radiation spectrum by $0.5 - 1\%$ according to simple relation $\Delta\omega/\omega = 2\Delta E/E$. Another consequence of the energy chirp is suppression of the FEL gain. The merit of the influence of the energy chirp on the gain is $(\rho E/\tau_{\rm c})^{-1}\, {\rm d}\, E/\, {\rm d}\, t$. It becomes to play significant role when relative energy change on a scale of coherence length $c\tau_{\rm c}$ becomes to be comparable with FEL parameter ρ [10]. This effect is not small in the case under study, and results in significant correction to the FEL gain within the leading current spike. Suppression of the gain is stronger when slice current becomes to be less. In the high gain linear regime the effect of energy chirp leads to further shortening of the lasing part of the electron bunch. Estimations show that with all effects taken into account the lasing part of the electron bunch is only 3-5 times larger than coherence length. As a result, we can expect specific features of the radiation from SASE FEL driven by ultra-short electron bunch [11]. These features are: ultra-short radiation pulse duration (comparable with coherence length), and strong suppression of the energy fluctuations in the nonlinear regime.

We see that physical effects influencing operation of VUV FEL in the femtosecond regime are rather transparent. However, quantitative description of the output radiation can be obtained only with numerical simulations. To extract more detailed information about radiation properties, we performed 500 statistically independent runs with three-dimensional, time-dependent FEL simulation code FAST [12]. The result of each run contains parameters of the output radiation (amplitude and phase) stored on three-dimensional mesh. At the next stage of the numerical experiment the data arrays are handled with postprocessor codes to extract different properties of the SASE FEL radiation such as averaged values, spectra, and statistical distributions.

4 Temporal structure of the radiation

Figures 5 and 6 show evolution of temporal structure of the radiation pulse (single pulse and averaged) along the undulator. Analysis of these results tells us that we deal with nonstationary process of light amplification which occurs due to short duration of lasing part of the electron bunch. Note that in the linear mode of operation we obtain significant suppression of the radiation in the tail of the pulse. Actually, there are two effects leading to the sharp decrease of the gain. The first one is decrease of the current. And the second effect, as we mentioned above, is the energy chirp along the electron bunch.

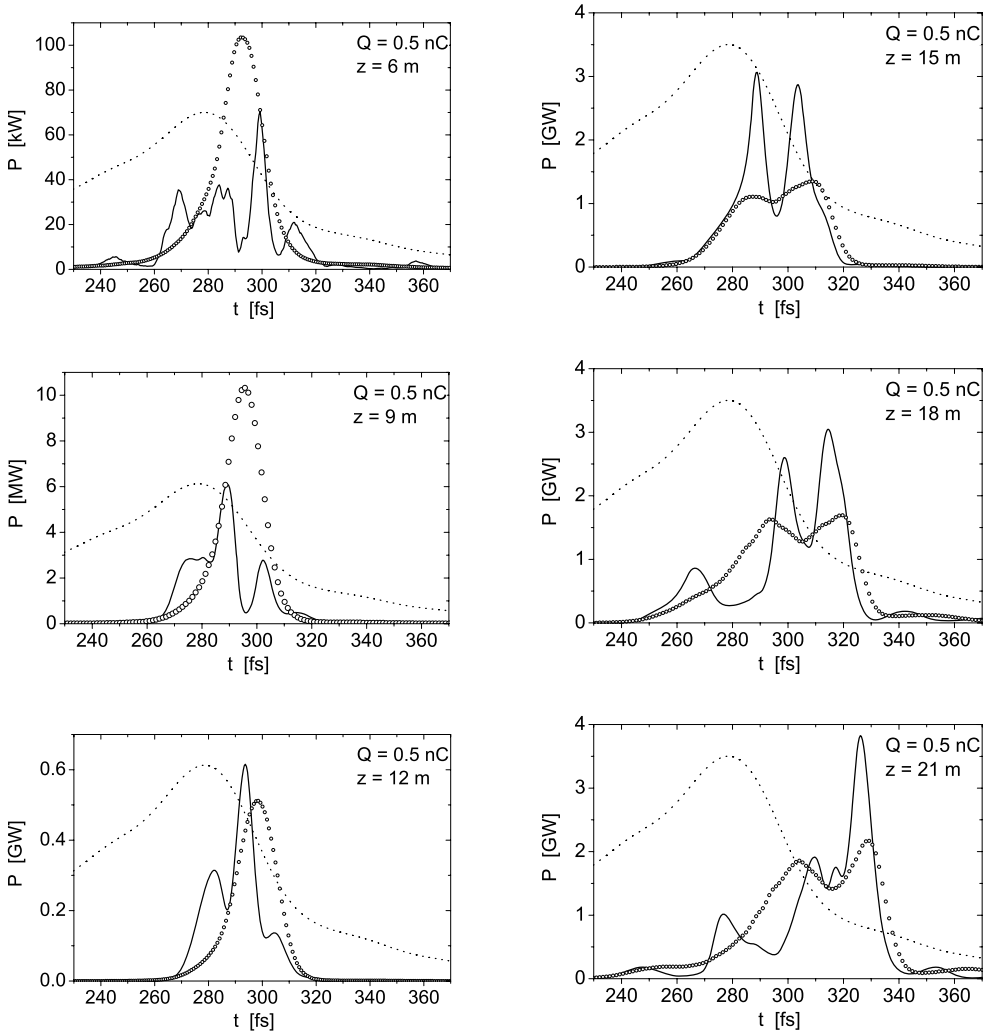

Fig. 5. Evolution of temporal structure of the radiation pulse. along the undulator. Solid and circles correspond to a single pulse and circles averaged profile, respectively. Left and right columns correspond to linear and nonlinear mode of operation, respectively. Bunch charge is 0.5 nC. Dashed line shows profile of the electron bunch. Bunch head is at the right side

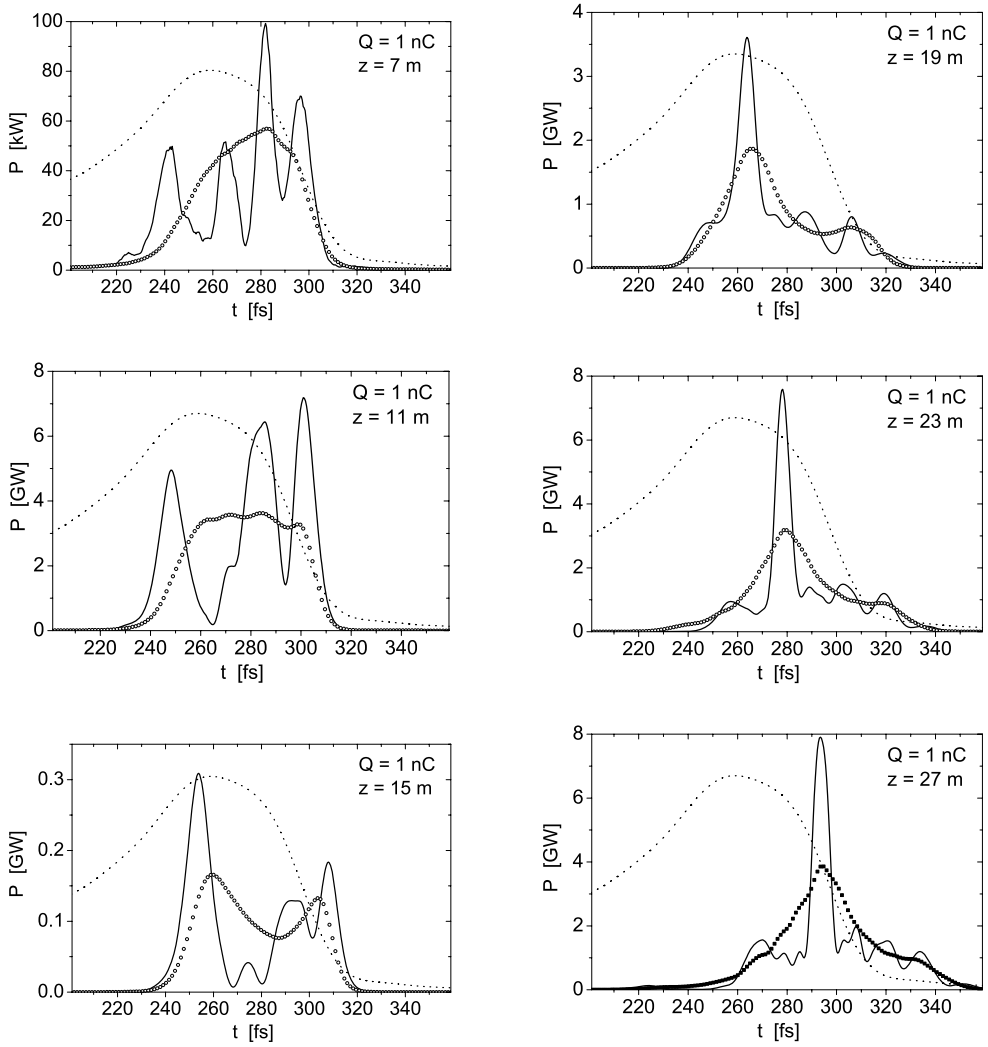

Fig. 6. Evolution of temporal structure of the radiation pulse. along the undulator. Solid line and circles correspond to a single pulse and averaged profile, respectively. Left and right columns correspond to linear and nonlinear mode of operation, respectively. Bunch charge is 1 nC. Dashed line shows profile of the electron bunch. Bunch head is at the right side

Its influence grows strongly when the current drops down. Thus, only half of the electron spike contribute to the light amplification in the linear regime. Numerical simulations shows that in the end of the linear regime the VUV FEL driven by 0.5 nC electron bunches produces short, down to 20 fs (FWHM) radiation pulse. VUV FEL driven by 1 nC bunch produces twice longer pulses. The reason for this is that 0.5 nC bunch has more narrow lasing part than 1 nC bunch (see Fig. 4). It is relevant to note that ultra-short pulse duration of 20 fs occurs not only due to ultra-short duration of the lasing part of the electron bunch. Another effect is suppression of the slippage effect in the linear regime [14]. In the free electron laser we deal with the wave propagating not in the free space, but with the wave which dynamically interacts with the electron

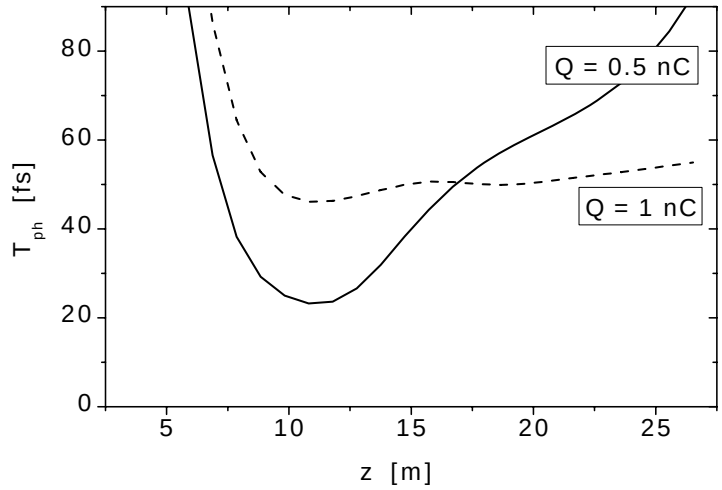

Fig. 7. Evolution of the FWHM radiation pulse length along undulator. Solid and dashed line correspond to the charge of 0.5 and 1 nC, respectively

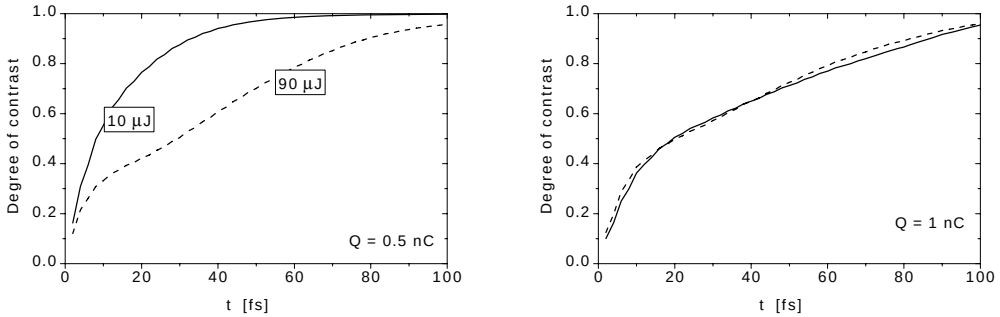

Fig. 8. Degree of contrast versus time gate around a spike with maximum intensity. Left: bunch charge is 0.5 nC. right: bunch charge is 1 nC. Solid and dashed line corresponds to the end of the linear regime and deep nonlinear regime, respectively

bunch. Slippage of the electromagnetic wave with respect to the electron beam is given by the value of the group velocity, $v_{\mathrm{g}} = \mathrm{d}\,\omega/\,\mathrm{d}\,k$. Group velocity of the electromagnetic wave in the high gain FEL regime is less than velocity of light c, and this results in significant reduction of the slippage (about factor of 3 in our case) [14].

In the linear mode of operation pulse duration is permanently reduced with the undulator length. When amplification process enters nonlinear stage, we obtain opposite situation. Radiation pulse lengthening occurs mainly due to two effects. First, suppression of the group velocity in the nonlinear regime becomes to be much less than in the high gain linear regime. Thus, radiation starts to slip forward faster. Second, the tail of the electron bunch starts to

produce visible amount of radiation. As a result we find that in the nonlinear regime the 0.5 nC case has no benefit in terms of pulse duration. Figure 7 shows evolution of the FWHM pulse length along the undulator. It is seen that shortest pulse duration occurs in the end of linear regime when average radiation energy is about a few μJ.

For the experiments utilizing the property of ultra short radiation pulse duration it is important to know the degree of contrast of the radiation pulse. The figure of merit for the degree of contrast is the ratio of the radiation energy within a time window τ around a spike with maximum peak power to the total energy in the radiation pulse:

$$C(\tau) = \frac{\int_{-\tau/2}^{\tau/2} P(t)\,\mathrm{d}\,t}{\int_{-\infty}^{\infty} P(t)\,\mathrm{d}\,t}\ . \tag{2}$$

The results for the average degree of contrast shown in Fig. 8 have been derived from 500 statistically independent runs. For fixed time window τ around the spike with maximum intensity we calculate the value of $C(\tau)$ for each pulse and then perform averaging over ensemble. Solid and dashed curves in Fig. 8 correspond to the end of the linear regime and deep nonlinear regime, respectively. We see that considered modes of the VUV FEL operation (driven by bunches with 0.5 nC and 1 nC charge) provide quite different properties for the contrast of the radiation pulse. The VUV FEL driven by 0.5 nC bunch is capable to produce short, down to 20 fs radiation pulses with GW-level peak power and contrast of 80%. This happens due to shorter lasing part of the bunch. Maximum contrast of the radiation pulses occurs in the end of the linear mode of operation. Average energy in the radiation pulse is about 10 μJ in this case. Increase of the radiation energy above this value leads to gradual decrease of the contrast due to radiation pulse lengthening in the nonlinear regime. The case of 1 nC demonstrate the contrast of the radiation pulse nearly independent on the pulse energy: 80% at 50 fs.

5 Temporal correlation functions

The shot noise in the electron beam causes fluctuations of the beam density which are random in time and space. As a result, the radiation, produced by such a beam, has random amplitudes and phases in time and space. Figures 5 and 6 show examples of single radiation pulse in terms of radiation power. Qualitative analysis of these plots allows to estimate coherence time of the radiation, but complete description of coherence properties can be obtained only in terms of correlation functions. Radiation from SASE FEL has a narrow band around resonant frequency ω, and electric field of the wave can be

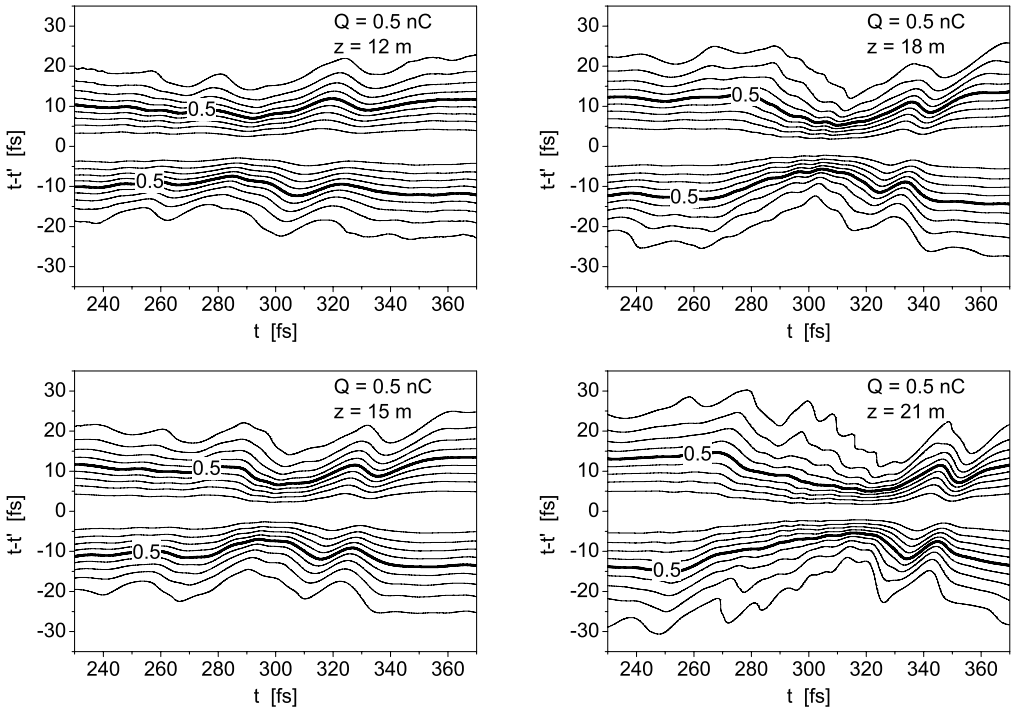

Fig. 9. Contour plot of the module of the first order correlation function for different undulator length. Bold lines trace the FWHM level. Bunch charge is 0.5 nC. Time interval corresponds to that of temporal structure shown in Fig. 5. Bunch head is at the right side

presented as

$$E_y(z,t) = \tilde{E}(z,t)e^{\mathrm{i}\,\omega_0(z/c-t)} + \text{C.C.}\ , \tag{3}$$

where $\tilde{E}(z,t)$ is slowly varying amplitude. In the case under study we deal with non-stationary random process, and use general definition for the first-order time correlation function:

$$g_1(t,t') = \frac{\langle \tilde{E}(t)\tilde{E}^*(t')\rangle}{\left[\langle|\tilde{E}(t)|^2\rangle\langle|\tilde{E}(t')|^2\rangle\right]^{1/2}}\ . \tag{4}$$

Here $\langle\ldots\rangle$ means averaging over ensemble (shots). Numerical simulation code produces arrays for complex amplitudes for the slowly varying amplitude of the radiation field in the near zone. Then we propagate this field into the far zone, and calculate coherence properties for the radiation field at zero observation angle. Statistical accuracy of 500 events is sufficient for reliable description of correlation functions. Figures 9 and 10 show the evolution of the first order correlation function from the end of linear regime down to deep nonlinear regime. Bold lines trace the FWHM level. Time window of the plots

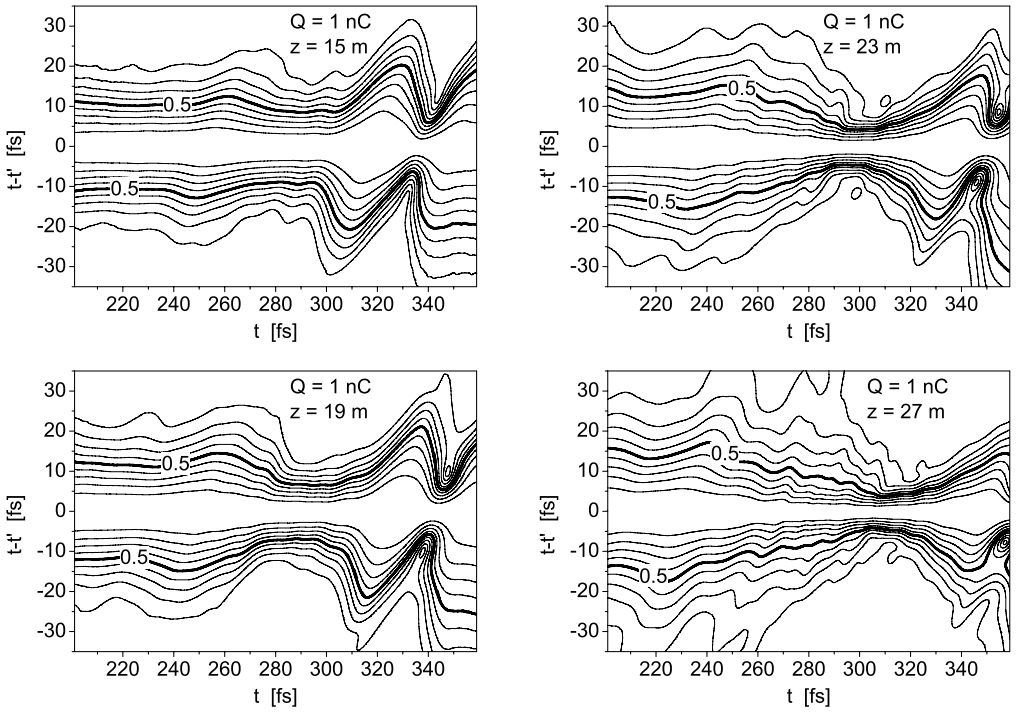

Fig. 10. Contour plot of the module of the first order correlation function for different undulator length. Bold lines trace the FWHM level. Bunch charge is 1 nC. Time interval corresponds to that of temporal structure shown in Fig. 6. Bunch head is at the right side

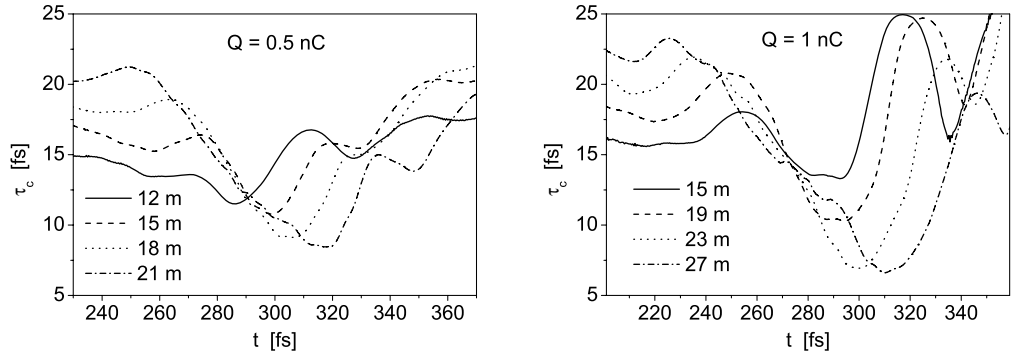

Fig. 11. Coherence time τ_c along the radiation pulse for different undulator length. Left and right columns correspond to the of 0.5 and 1 nC, respectively. Time interval corresponds to that of temporal structure shown in Figs. 5 and 6. Bunch head is at the right side

is the same as for temporal structure of the radiation shown in Figs. 5 and 6. Following general definition we calculate coherence time as

$$\tau_c(t) = \int_{-\infty}^{\infty} |g_1(t,t')|^2 \, \mathrm{d}\, t' \ . \tag{5}$$

Figure 11 shows coherence time $\tau_c(t)$ along the radiation pulse for different undulator length. Calculation are performed from the data shown in Figs. 9 and 10. We see that behavior of the correlation function and correlation time along the radiation pulse is rather complicated. From practical point of view the value of interest is the coherence time in the core of the radiation pulse (maximum of the averaged radiation power). We see that coherence time for the core of the radiation pulse has maximum value in the end of the linear regime (solid line), and drops down gradually when amplification process enters deep nonlinear regime (dash-dot line). Such a behavior is quite natural, and is well known from studies of SASE FEL driven by long pulses [14,15]. Origin of the reduction of coherence time is in the growth of the sidebands in the nonlinear media.

6 Statistics of the radiation energy

Figure 12 shows average energy in the radiation pulse and rms fluctuations as functions of position along the undulator. Expected level of the output energy at saturation is approximately the same for 0.5 and 1 nC bunch charge, of about 100 μJ, while the saturation length is a little bit shorter for the case of 0.5 nC. More pronounced difference is in the behavior of the fluctuations of the radiation energy. Plots presented in Fig. 12 show the value $\sigma_E = \sqrt{\langle (E - \langle E \rangle)^2 \rangle}/\langle E \rangle$. These fluctuations reach maximum value in the end of the linear regime. It is known that the radiation from SASE FEL operating in the linear regime possesses properties of completely chaotic polarized light [14,15]. One important property is that probability distribution of the

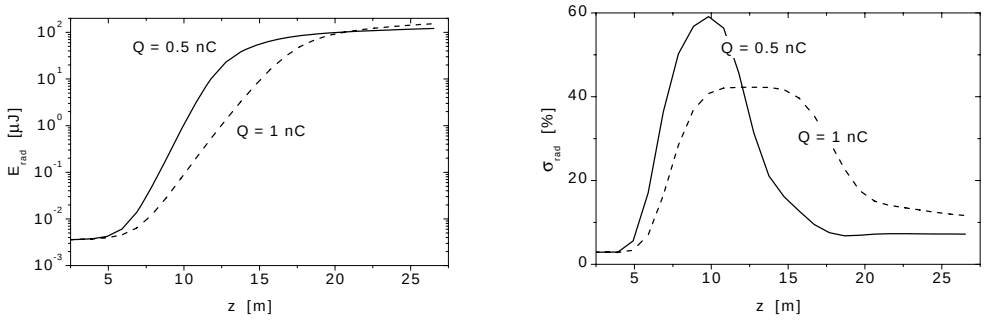

Fig. 12. Average energy in the radiation pulse (left plot) and fluctuations of the energy in the radiation pulse (right plot) versus undulator length. Solid and dashed lines refer to bunch charge 0.5 nC and 1 nC, respectively

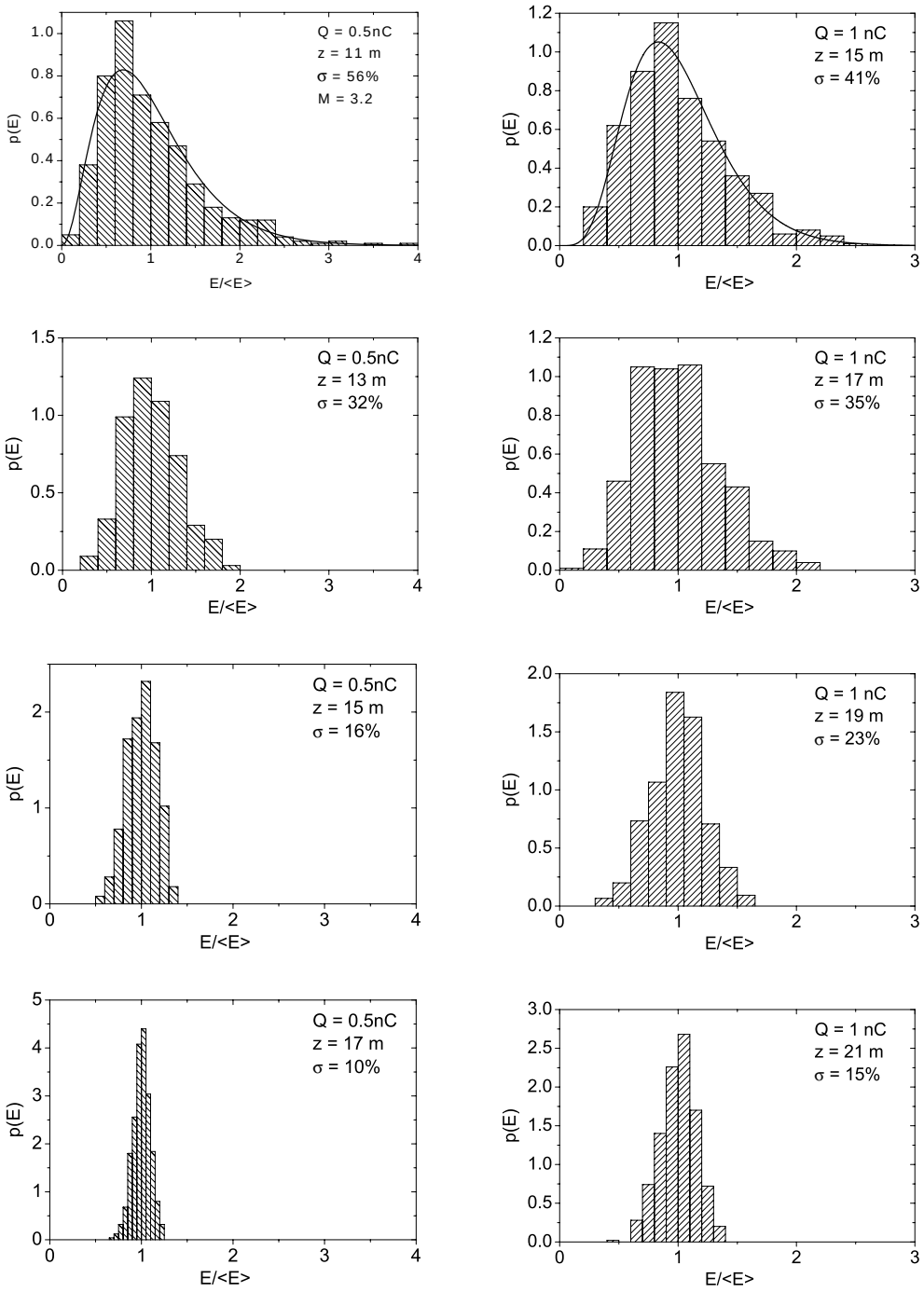

Fig. 13. Evolution of the probability distribution from end of the linear regime down to deep nonlinear regime. Left and right columns correspond to the case of 0.5 and 1 nC, respectively. Solid lines show gamma distribution

energy in the radiation pulse must follow gamma-distribution:

$$p(E) = \frac{M^M}{\Gamma(M)} \left(\frac{E}{\langle E \rangle}\right)^{M-1} \frac{1}{\langle E \rangle} \exp\left(-M \frac{E}{\langle E \rangle}\right) \ , \tag{6}$$

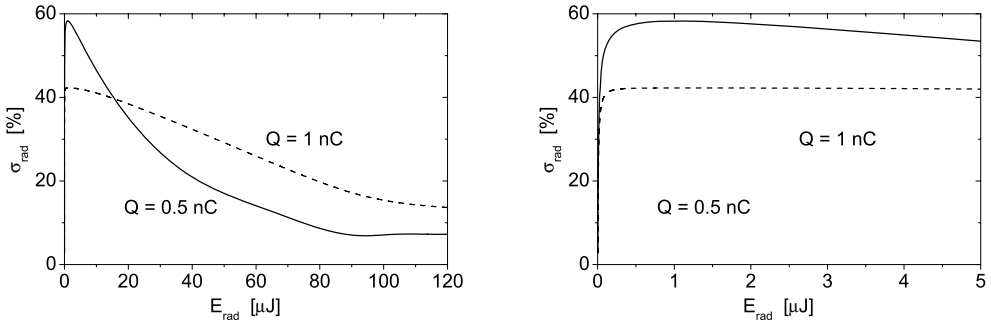

Fig. 14. Fluctuations of the energy in the radiation pulse versus average energy in the radiation pulse. Right plot shows zoomed area of the left plot. Solid and dashed lines refer to bunch charge 0.5 nC and 1 nC, respectively

where $\Gamma(M)$ is the gamma function, and $M = 1/\sigma_E^2$. The parameter M can be interpreted as the average number of "degrees of freedom" or "modes" in the radiation pulse. According to Fig. 12 number of modes for the VUV FEL is expected to be in the range $3 - 6$. Smaller number of modes for the case of 0.5 nC is clear indication for shorter pulse duration.

Amplification process in the SASE FEL starts from shot noise in the electron beam, and the radiation pulse initially consists of a large number of longitudinal and transverse modes. In the linear stage of amplification the number of transverse modes in the radiation pulse drops down due to the mode selection process. First this process passes the stage exponential decay, and then asymptotically approaches to single-mode case. Final degree of transverse coherence is limited by finite spectrum width of the SASE FEL [16]. The number of longitudinal modes in the end of the linear is settled proportionally to the ratio of the length of the lasing part of the bunch to the coherence length. Thus, in the linear regime we occur permanent reduction of the number of radiation modes which leads to growth of the fluctuations of the radiation energy (see Fig. 12).

Fluctuations of the radiation energy change drastically when amplification process enters the nonlinear regime. One can see from Fig. 12 that fluctuations of the radiation energy drop down on a scale of about one gain length. Note that such a fast drop of fluctuations is the feature of ultra-short pulse duration [11]. Nature of this phenomenon can be understood by analyzing structure of the radiation pulse (see Figs. 5 and 6). When amplification process enters nonlinear stage, group velocity of the radiation becomes to be close to the velocity of light, and saturated wavepackets start to slip forward with respect to the electron bunch. Further growth of the total radiation energy occurs due to the radiation of the bunched electron beam. Since maximum bunching of the electron beam is limited to the unity, this additional radiation is well stabilized, leading to the overall stability of the total energy in the radiation pulse.

Figure 13 presents evolution of the probability distributions of the radiation energy along the undulator As we mentioned above the radiation from SASE FEL operating in the linear regime possesses properties of completely chaotic polarized light [14,15]. In particular, an important property is that probability distribution of the energy in the radiation pulse must follow gamma-distribution (6). In the nonlinear regime probability distributions change significantly. Specific shape of the distribution becomes to be dependent on undulator length and details of the lasing part of the electron bunch (temporal profile of current, energy, emittance). However, we note one specific feature of the distributions: in the nonlinear regime they exhibit an asymmetry with a tail spanning to lower radiation energies. Somehow the shape looks like an mirrored gamma distribution. Similar qualitative behavior has been obtained also at the VUV FEL, phase I, in the simulations and in the experiment as well [5,17]. Our experimental experience is that this feature can be used as an effective tool for reliable detection of the nonlinear regime even in the case of strong fluctuations of machine parameters.

One more practically important result can be derived from the data shown in Fig. 12. This is the dependency of fluctuations of the energy in the radiation pulse versus average energy in the radiation pulse (see Fig. 14). Note that this dependency is not affected strongly by imperfections of the machine parameters. The first order effect of machine imperfections is the gain length which is excluded from the relation between fluctuations and average energy. Thus, measuring energy fluctuations in the linear regime and in the nonlinear regime we can derive rather precise on-line estimation for the average energy in the radiation pulse.

7 Spectral properties of the radiation

Figures 15 and 16 show evolution of the radiation spectra along the undulator. Single-shot spectra are derived from the data shown in Figs. 5 and 6. The reference energy for the resonance frequency corresponds to the maximum of the peak current (see Fig. 4). Calculation for a slice corresponding to maximum of current spike gives the value for the FEL parameter $\rho = 2.5 - 3 \times 10^{-3}$ for maximum of peak current (see Fig. 4). Thus, spectrum width generated by a slice of the electron beam is expected to be about $\Delta\omega/\omega \simeq 2\rho \simeq 0.5 - 0.6\%$. Calculated spectrum width is visibly wider. The origin of this phenomenon is in strong energy chirp along the lasing fraction of the bunch. Using data from Fig. 4 we can easily estimate extra widening of the radiation spectrum by $0.5 - 1\%$ according to simple relation $\Delta\omega/\omega = 2\Delta E/E$. In particular, more wide spectrum for the case of 1 nC is due to larger energy chirp with respect to 0.5 nC case.

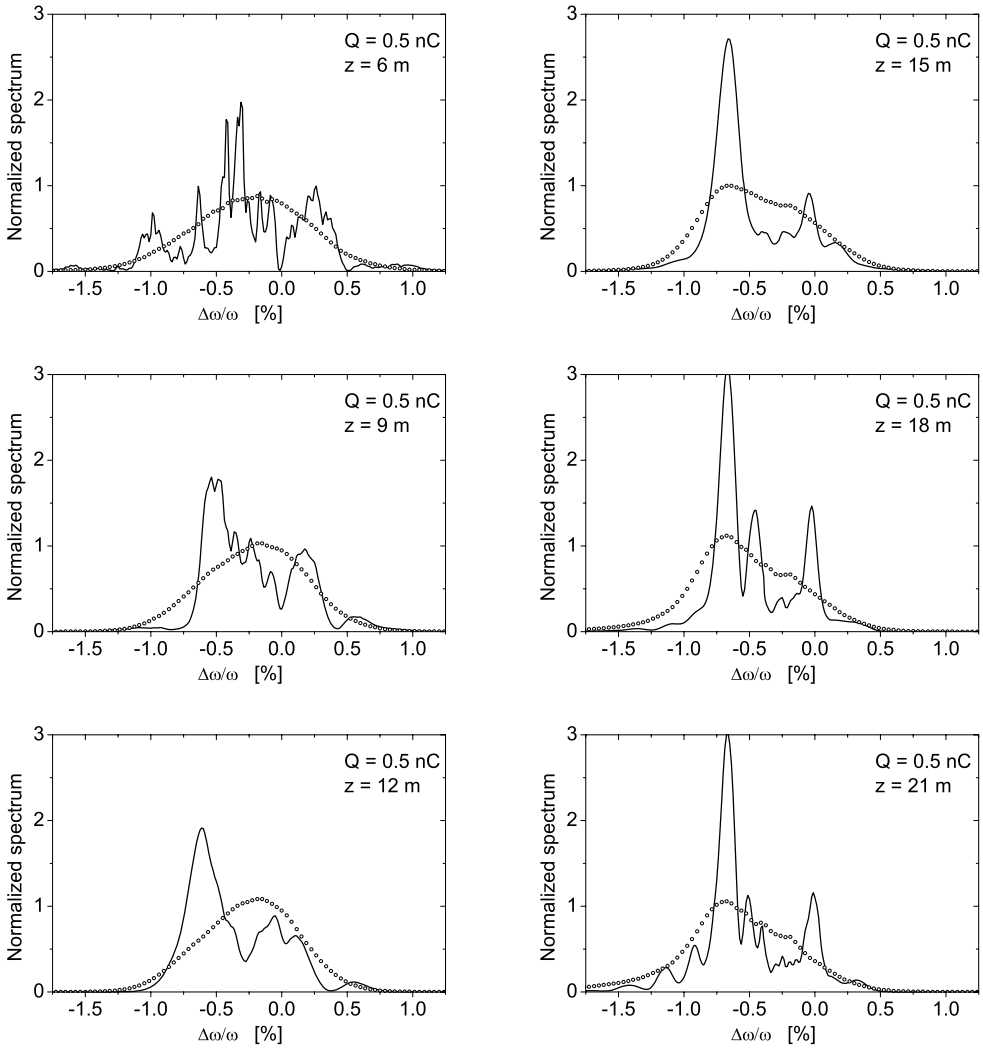

Fig. 15. Evolution of spectral structure of the radiation pulse along the undulator. Solid line and circles correspond to a single pulse and averaged profile, respectively. Left and right columns correspond to linear and nonlinear mode of operation, respectively. Bunch charge is 0.5 nC

Another subject is statistics of SASE FEL radiation filtered through narrowband monochromator. In the linear stage of SASE FEL operation the value of normalized energy deviation is equal to unity, and energy fluctuates in accordance with negative exponential distribution:

$$p(E) = \exp\left(-\frac{E}{\langle E\rangle}\right) \ . \tag{7}$$

This is consequence of the fact that the radiation from SASE FEL operating in the linear regime is gaussian random process. This property remains valid for any pulse length. When amplification process enters nonlinear stage

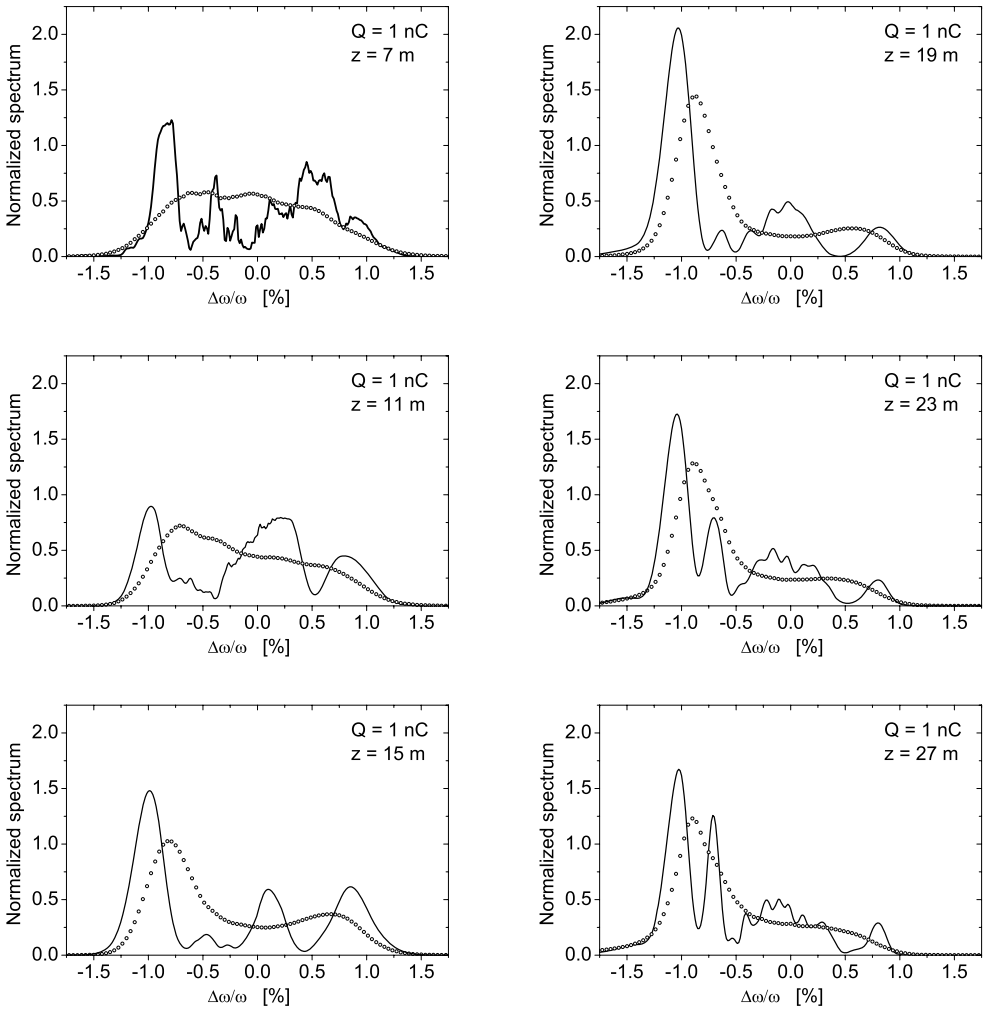

Fig. 16. Evolution of spectral structure of the radiation pulse along the undulator. Solid line and circles correspond to a single pulse and averaged profile, respectively. Left and right columns correspond to linear and nonlinear mode of operation, respectively. Bunch charge is 1 nC

the radiation is not gaussian random process anymore due to the process of sideband growth in the nonlinear media. In particular, the probability distribution of the total radiation energy does not follow gamma distribution anymore as it was shown in the previous section. Situation with probability distribution of the radiation energy after narrow band monochromator is more complicated. Earlier studies have shown that in the case of long radiation pulse (much longer than coherence length) property of the negative exponential distribution remains to be valid in the nonlinear regime as well [14,15]. Situation changes dramatically when pulse duration becomes to be short, of about coherence length. Recent studies have shown that in this case an effect of strong suppression of the fluctuations of the radiation energy after narrow band monochromator is expected [11]. Later on this effect has been measured

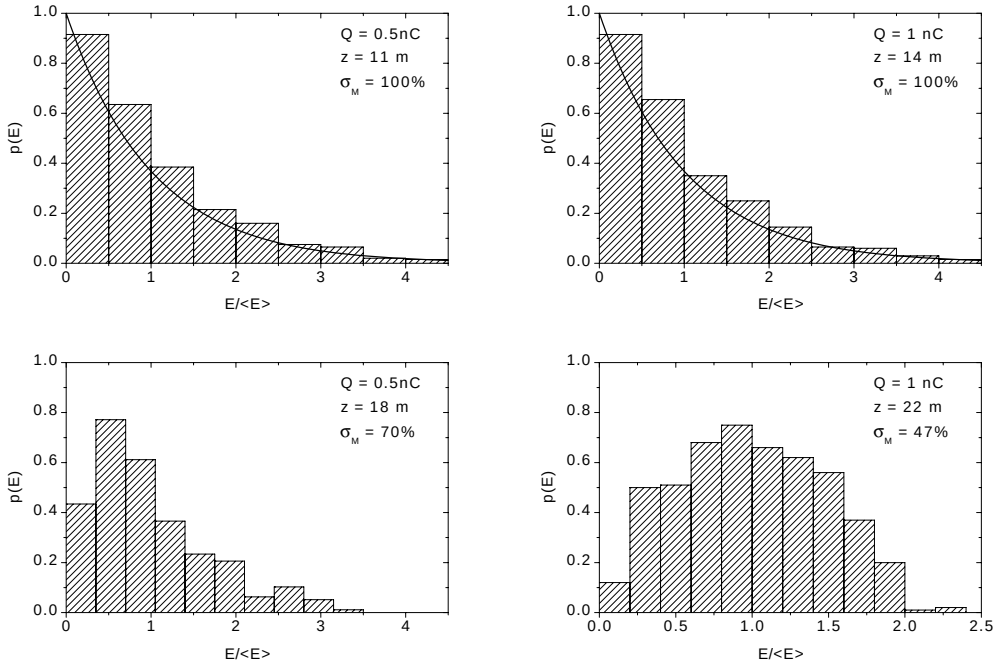

Fig. 17. Probability distribution of the energy in the radiation pulse after narrow band monochromator. Top and bottom plots correspond to linear regime and saturation, respectively. Left column: bunch charge is 0.5 nC. Right column: bunch charge is 1 nC. Solid line shows negative exponential distribution

experimentally at the VUV FEL, phase I [17]. Our simulations show that suppression of the fluctuations is expected for the VUV FEL as well (see Fig. 17). This effect has simple physical explanation [11]. Let us consider an extreme case of SASE FEL driven by an electron bunch of about coherence length. For this extreme case each radiation pulse consists of a single spike only. For different shots the radiation pulses have similar shape, but amplitude fluctuates nearly by negative exponential distribution. When amplification process enters nonlinear stage, amplitudes of different pulses are equalized due saturation effects, while keeping close shape. Spectrum of the radiation pulse is given by Fourier transform of the radiation field, and at saturation we obtain nearly similar spectrum envelope for different pulses. As a result, we can expect that fluctuations of the radiation energy after narrow-band monochromator should follow fluctuations of the total energy in the radiation pulse which drop down drastically. For longer radiation pulses suppression is not so strong and nearly vanishes for the bunches longer than four coherence length. In the case under study the lasing part of the bunch is about 2-3 times longer than coherence length.

8 An overview of the first experimental results

This work (statistical calculations of the radiation properties) has been performed in parallel with the first run of the VUV FEL. The range of optimum tuning of the VUV FEL proposed in [6] and described here has been chosen for the commissioning of the VUV FEL. A consistent set of experimental data has been recorded for the case when VUV FEL has been driven by electron bunches with 1 nC charge. Average energy in the radiation pulse was equal to 1 μJ which corresponds to the high gain linear regime [7].

Plot on the left side of Fig. 18 shows measured values of the radiation energy versus time. Corresponding probability distribution derived from experimental data is shown on the right plot. We see that experimentally measured distri-

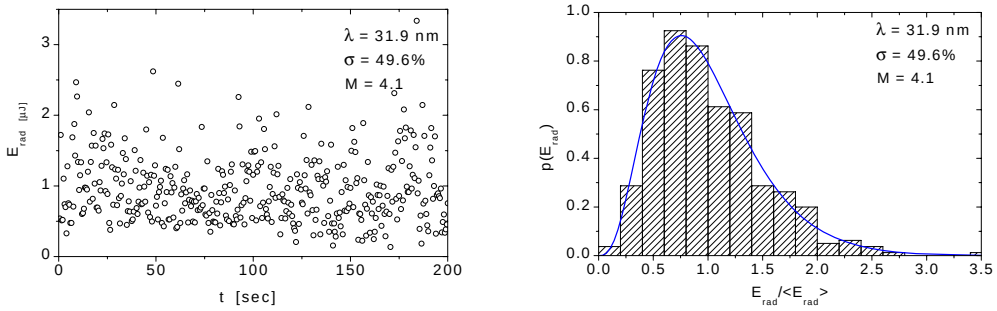

Fig. 18. Experimental results from the VUV FEL. Measurements of the energy in the radiation pulse. VUV FEL operates in the linear regime. Left plot – measured energy versus time. Right plot – probability distribution of the radiation energy. Solid curve represents gamma distribution

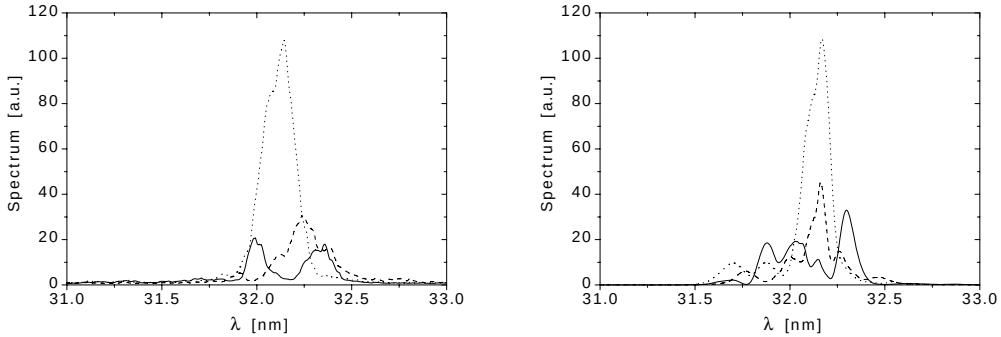

Fig. 19. Experimental results from the VUV FEL. Left: Single-shot spectra of radiation pulses (experimental results). Right: simulation of spectral structure of the radiation pulse from VUV FEL operating in the linear regime at the undulator length of 13 m [6]

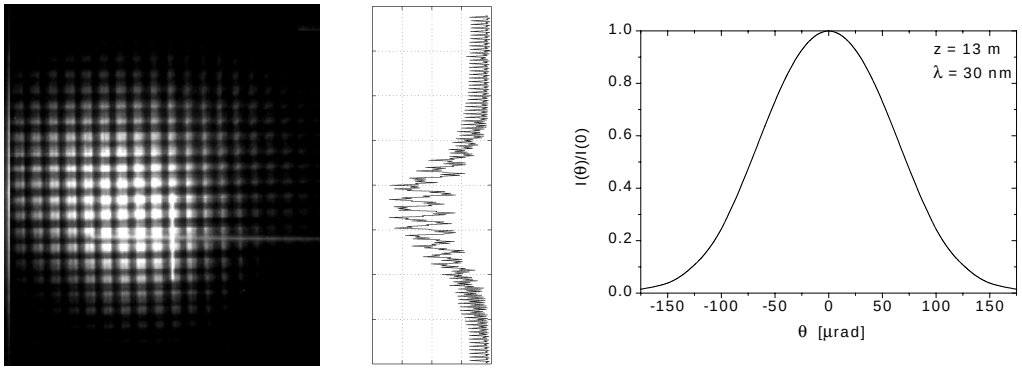

Fig. 20. Experimental results from the VUV FEL. Left plot: image on CeYaG crystal of a single-shot VUV FEL pulse passed through gold mesh of the radiation detector placed 18.5 m downstream undulator exit. Distance between wires in the mesh is 0.25 mm, wire diameter is 60 μm. Image analysis (middle plot) gives FWHM spot size of 3 mm which corresponds to FWHM angular divergence of 160 μrad. Right plot: simulated angular distribution of the radiation intensity in the far zone [6]

bution follows well gamma distribution with parameter $M = 4.1$ derived from experimental data as $M = 1/\sigma_E^2$. Note that measured fluctuations are mainly fundamental fluctuations due to start-up of the FEL process from the shot noise. Contribution of machine fluctuations is estimated to be less than 10%. Measured value for the number of modes in the radiation pulse is consistent with theoretical prediction (see Fig. 12).

Spectral measurements are presented in Fig. 19 [7]. Single-shot spectra were taken with a monochromator (0.04 nm resolution) equipped with an intensified CCD camera [18]. Analysis of measured spectra shows that there is good agreement with early theoretical predictions [6] (see right plot in Fig. 19). Ultra-short pulse duration does not allow direct measurements of temporal structure of single pulses, but measurements of single-pulse spectra are possible. Monochromator performs Fourier transform of the radiation pulse. Despite the phase is missed in such measurements, they still contain an essential information about primary object. In fact, average number of spikes in the single-shot spectra should correspond to average number of spikes in the temporal structure. Thus, visual analysis of single shot spectra allows us to derive a zero-order estimate for the number of longitudinal modes. Since monochromator acts as a Fourier transformation, we can state that typical width of the spike in the spectrum $\Delta\omega$ should be inversely proportional to the radiation pulse duration. Using the relation $\tau_{\rm rad} \sim 2\pi/(\Delta\omega)$ we can give an estimation for the pulse duration. Measured spike widths presented correspond to the radiation pulse length $20-40$ fs which is in a good agreement with theoretical results.

Figure 20 shows an image on CeYaG crystal of a single-shot VUV FEL pulse passed through a gold mesh of the radiation detector placed 18.5 m down-

stream undulator exit [19]. Distance between the centers of wires in the mesh is 0.31 mm. Image analysis gives FWHM spot size of 3 mm which corresponds to FWHM angular divergence of 160 μrad. Right plot shows simulated angular distribution of the radiation intensity in the far zone [6]. We find good agreement between simulated and experimental data.

Measurements of angular divergence provide valuable information about the degree of transverse coherence. FWHM spot size of the photon beam at the undulator exit is about 250 μm [6]. One can easily calculate that product of the spot size of the radiation at the undulator exit by measured angular divergence results in the value of about radiation wavelength. This means that the phase volume of the radiation is close to diffraction limit, and the radiation from the VUV FEL has high degree of transverse coherence.

9 Summary

An important lesson from our study and the first operation of the VUV FEL is that GW-level, laser-like VUV radiation pulses on a sub-50 fs scale are produced with a simple and reliable single-pass SASE FEL scheme. The generation of ultra-short radiation pulses became possible due to specific tailoring of the bunch charge distribution. Such a technique is more reliable and effective with respect to sophisticated HGHG schemes widely discussed as a future alternative to single-pass SASE FEL in terms of shorter pulse duration and better quality of output radiation (see, e.g. [20] and references therein). Key element of the VUV FEL operating in the femtosecond regime is nonlinear bunch compression scheme producing tailored electron bunches with a short high-current leading peak in the density distribution that produces FEL radiation. An important feature of the beam formation system is strong influence of collective effects. One of them, longitudinal space charge, plays an extremely important role: induced energy chirp along the lasing part of the bunch allows further shortening of the lasing fraction of the electron bunch. As a result, it becomes possible to generate ultra-short, down to 20 fs radiation pulses with GW-level peak power and contrast of 80%.

Acknowledgments

We are grateful to J.R. Schneider for interest in this work and stimulating discussions.

References

[1] The TTF FEL team, DESY Print TESLA-FEL 2002-01, June 2002.

[2] V. Ayvazyan et al., Phys. Rev. Lett. 88(2002)104802.

[3] V. Ayvazyan et al., Eur. Phys. J. D20(2002)149.

[4] T. Åberg, et al., A VUV FEL at the TESLA Test Facility at DESY, Conceptual Design Report, DESY Print TESLA-FEL 95-03 , May 1995.

[5] M. Dohlus et al., Nucl. Instrum. and Methods A530(2004)217.

[6] E.L. Saldin, E.A. Schneidmiller, M.V. Yurkov, DESY Print TESLA-FEL 2004-06, July 2004.

[7] V. Ayvazyan et al., Eur. Phys. J. D **37**(2006)297.

[8] K. Flöttmann, S.M. Lidia, and P. Piot, Proc. 2003 Particle Accelerator Conference, p. 3500.

[9] M. Borland, "`elegant`: A flexible SDDS-Compilant Code for Accelerator Simulation", APS LS-287, September 2000.

[10] E.L. Saldin, E.A. Schneidmiller and M.V. Yurkov, Proceedings of the 27th Int. Free Electron Laser Conference, p. 258.

[11] E.L. Saldin, E.A. Schneidmiller and M.V. Yurkov, Nucl. Instrum. and Methods **A507**(2003)101.

[12] E.L. Saldin, E.A. Schneidmiller and M.V. Yurkov, Nucl. Instrum. and Methods **A429**(1999)233.

[13] R. Bonifacio, C. Pellegrini and L.M. Narducci, Opt. Commun. **50**(1984)373.

[14] E.L. Saldin, E.A. Schneidmiller, M.V. Yurkov, "The Physics of Free Electron Lasers" (Springer-Verlag, Berlin, 1999).

[15] E.L. Saldin, E.A. Schneidmiller and M.V. Yurkov, Opt. Commun. **148**(1998)383.

[16] E.L. Saldin, E.A. Schneidmiller and M.V. Yurkov, Opt. Commun. **186**(2000)185.

[17] V. Ayvazyan et al., Nucl. Instrum. and Methods **A507**(2003)368-372.

[18] R. Treusch et al., Nucl. Instrum. and Methods **A467-468**(2001)30.

[19] A. Bytchkov et al., Nucl. Instrum. and Methods A528(2004)254.

[20] G. Lambert et al., Proc. FEL 2005 Conference (Trieste, Italy, 2004), p.155.